

Modern Physics Letters A
 © World Scientific Publishing Company

$l_\alpha \rightarrow 3l_\beta$ in Minimal R-symmetric Supersymmetric Standard Model

Ke-Sheng Sun ^{a,*}, Jian-Bin Chen ^{b,*}, Hai-Bin Zhang ^{c,†}, Sheng-Kai Cui ^{c,‡}

^a *Department of Physics, Baoding University, Baoding 071000, China*

^b *College of Physics and Optoelectronic Engineering, Taiyuan University of Technology, Taiyuan 030024, China*

^c *Department of Physics, Hebei University, Baoding 071002, China*

* *sunkesheng@126.com; sunkesheng@mail.dlut.edu.cn*

* *chenjianbin@tyut.edu.cn*

† *hbzhang@hbu.edu.cn*

‡ *2252953633@qq.com*

Received (Day Month Year)

Revised (Day Month Year)

Lepton flavor violation decays are channels which may lead to fundamental discoveries in the forthcoming years and this make it an exciting research field for beyond the Standard Model searches. In this work, we present an analysis of the lepton flavor violation decays $l_\alpha \rightarrow 3l_\beta$ in Minimal R-symmetric Supersymmetric Standard Model. The prediction for $\text{BR}(l_\alpha \rightarrow 3l_\beta)$ depend on the off-diagonal entries of the slepton mass matrix. The contributions to Wilson coefficients can be classified into Higgs penguins, photon penguins, Z penguins, and box diagrams. It shows the contribution from Z penguins dominates the predictions for $\text{BR}(l_\alpha \rightarrow 3l_\beta)$, and the contributions from Higgs penguins and box diagrams play different roles in different decay channels. The theoretical predictions for $\text{BR}(l_\alpha \rightarrow 3l_\beta)$ can reach the future experimental limits, and there channels are very promising to be observed in near future experiment.

Keywords: R-symmetry; MRSSM; Lepton flavor violation

1. Introduction

Many efforts have been devoted to searching for Lepton Flavor Violation (LFV) decays in experiment and literature, since it is one of the signals for New Physics (NP) beyond the Standard Model (SM) in which the lepton flavor is conserved. The present upper bounds and future sensitivities for the LFV decays $l_\alpha \rightarrow 3l_\beta$ are summarized in Table.1. Several predictions for these LFV processes have obtained in the framework of various extended SM. One of the most attractive concepts for NP beyond SM is supersymmetry, which is the only possible nontrivial extension of the Poincaré algebra in a relativistic quantum field theory.

In this work, we will analyze these LFV decays in the Minimal R-symmetric Supersymmetric Standard Model (MRSSM). The MRSSM is proposed in Ref.¹ and gives a new solution to the supersymmetric flavor problem in MSSM, where the R-symmetry, being different from R-parity, is a fundamental symmetry proposed

several years ago^{2,3} and not present in models like the Minimal Supersymmetric Standard Models(MSSM). The continuous R-symmetry forbids Majorana gaugino masses, then the gaugino masses can not be anything but Dirac masses which leads to the gauge boson has a Dirac gaugino and a scalar superpartner. The R-symmetry also forbids μ term, A terms, and all left-right squark and slepton mass mixings. The R-charged Higgs $SU(2)_L$ doublets \hat{R}_u and \hat{R}_d are introduced in MRSSM to yield the Dirac mass terms of higgsinos. Additional superfields \hat{S} , \hat{T} and \hat{O} are introduced to yield Dirac mass terms of gauginos. Studies on phenomenology in MRSSM can be found in literatures^{4,5,6,7,8,9,10,11,12,13,14,15,16,17,18,19,20,21}.

Table 1. Present limits and future sensitivities for $\text{BR}(l_\alpha \rightarrow 3l_\beta)$.

LFV process	Present limit	Future sensitivity
$\mu \rightarrow 3e$	1.0×10^{-12} Ref. ²²	10^{-16} Ref. ²³
$\tau \rightarrow 3e$	2.7×10^{-8} Ref. ²⁴	$10^{-9} - 10^{-10}$ Ref. ²⁵
$\tau \rightarrow 3\mu$	2.1×10^{-8} Ref. ²⁴	$10^{-9} - 10^{-10}$ Ref. ²⁵

In SM, the LFV decays mainly originate from the charged current with the mixing among three lepton generations. The fields of the flavor neutrinos in charged current weak interaction Lagrangian are combinations of three massive neutrinos:

$$\mathcal{L} = -\frac{g_2}{\sqrt{2}} \sum_{l=e,\mu,\tau} \bar{l}_L(x) \gamma_\mu \nu_{lL}(x) W^\mu(x) + h.c.,$$

$$\nu_{lL}(x) = \sum_{i=1}^3 \left(U_{PMNS} \right)_{li} \nu_{iL}(x),$$

where g_2 denotes the coupling constant of gauge group $SU(2)$, ν_{lL} are fields of the flavor neutrinos, ν_{iL} are fields of massive neutrinos, and U_{PMNS} corresponds to the unitary neutrino mixing matrix^{26,27,28}.

In this paper, we have studied the LFV decays $l_\alpha \rightarrow 3l_\beta$ in MRSSM by considering the constraints on off-diagonal entries δ^{ij} from LFV decays $l_\alpha \rightarrow l_\beta \gamma$. We first consider an effective Lagrangian that includes the operators relevant for the flavor observable of $l_\alpha \rightarrow 3l_\beta$. Then, by taking into account all possible 1-loop topologies leading to the relevant operators, the Wilson coefficients are computed for each Feynman diagram, in which the contributions have been classified into four categories (Higgs, photon, Z, box). Finally, the results for the Wilson coefficients are plugged in a general expression for $\text{BR}(l_\alpha \rightarrow 3l_\beta)$ and a final result is obtained.

The paper is organized as follows. In Section 2, we firstly provide a brief introduction on MRSSM. Then, we derive the analytic expressions of the Wilson coefficients in each Feynman diagram contributing to $l_\alpha \rightarrow 3l_\beta$ in MRSSM in detail. The numerical results are presented in Section 3, and the conclusion is drawn in Section 4.

2. MRSSM

First, it is necessary to provide a simple introduction to MRSSM. In MRSSM, the spectrum of fields contain the standard MSSM matter, Higgs and gauge superfields augmented by chiral adjoints, two R-Higgs iso-doublets. The superfields with R-charge in MRSSM can be found in Ref.²⁰, which is not listed for simplicity. The general form of the superpotential in MRSSM is given by⁴

$$\begin{aligned} W_{MRSSM} = & \mu_d(\hat{R}_d H_d) + \mu_u(\hat{R}_u H_u) + \Lambda_d(\hat{R}_d \hat{T}) H_d \\ & + \Lambda_u(\hat{R}_u \hat{T}) H_u + Y_u \bar{U}(Q H_u) - Y_d \bar{D}(Q H_d) \\ & - Y_e \bar{E}(L H_d) + \lambda_d \hat{S}(\hat{R}_d H_d) + \lambda_u \hat{S}(\hat{R}_u H_u), \end{aligned} \quad (1)$$

where H_u and H_d stand for the MSSM-like Higgs weak iso-doublets, \hat{R}_u and \hat{R}_d stand for the R -charged Higgs $SU(2)_L$ doublets and the corresponding Dirac higgsino mass parameters are μ_u and μ_d . The Yukawa-like trilinear terms, which involve the singlet \hat{S} and the triplet \hat{T} , contain four parameters λ_u , λ_d , Λ_u and Λ_d . The triplet \hat{T} is given by

$$\hat{T} = \begin{pmatrix} \hat{T}^0/\sqrt{2} & \hat{T}^+ \\ \hat{T}^- & -\hat{T}^0/\sqrt{2} \end{pmatrix}. \quad (2)$$

The soft-breaking scalar mass terms are given by

$$\begin{aligned} V_{SB,S} = & m_{H_d}^2(|H_d^0|^2 + |H_d^-|^2) + m_{H_u}^2(|H_u^0|^2 + |H_u^+|^2) + m_{R_u}^2(|R_u^0|^2 + |R_u^-|^2) \\ & + m_{R_d}^2(|R_d^0|^2 + |R_d^+|^2) + (B_\mu(H_d^- H_u^+ - H_d^0 H_u^0) + h.c.) \\ & + \tilde{d}_{L,i}^* m_{q,ij}^2 \tilde{d}_{L,j} + \tilde{d}_{R,i}^* m_{d,ij}^2 \tilde{d}_{R,j} + \tilde{u}_{L,i}^* m_{q,ij}^2 \tilde{u}_{L,j} + \tilde{u}_{R,i}^* m_{u,ij}^2 \tilde{u}_{R,j} \\ & + \tilde{e}_{L,i}^* m_{l,ij}^2 \tilde{e}_{L,j} + \tilde{e}_{R,i}^* m_{r,ij}^2 \tilde{e}_{R,j} + \tilde{\nu}_{L,i}^* m_{l,ij}^2 \tilde{\nu}_{L,j} \\ & + m_S^2 |S|^2 + m_O^2 |O|^2 + m_T^2 (|T^0|^2 + |T^-|^2 + |T^+|^2). \end{aligned} \quad (3)$$

It is noted worthwhile that all trilinear scalar couplings involving Higgs bosons to squarks and sleptons are forbidden due to the R -symmetry. The soft-breaking Dirac mass terms of the singlet \hat{S} , triplet \hat{T} and octet \hat{O} take the form

$$V_{SB,DG} = M_D^B \tilde{B} \tilde{S} + M_D^W \tilde{W}^a \tilde{T}^a + M_D^O \tilde{g} \tilde{O} + h.c., \quad (4)$$

where \tilde{B} , \tilde{W} and \tilde{g} are usually MSSM Weyl fermions.

For convenience, we will use the notations in Ref.^{19,20} for the mass matrices and mixing matrices of neutralino, chargino, slepton and sneutrino. One can find the explicit expressions of these mass matrices and mixing matrices in Ref.^{19,20} and we will not listed them in following. In the basis $(\sigma_d, \sigma_u, \sigma_S, \sigma_T)$, the pseudo-scalar Higgs boson mass matrix takes a simple form

$$\mathcal{M}_{A^0}^2 = \begin{pmatrix} B_\mu \frac{v_u}{v_d} & B_\mu & 0 & 0 \\ B_\mu & B_\mu \frac{v_d}{v_u} & 0 & 0 \\ 0 & 0 & m_S^2 + \frac{\lambda_d^2 v_d^2 + \lambda_u^2 v_u^2}{2} & \frac{\lambda_d \Lambda_d v_d^2 - \lambda_u \Lambda_u v_u^2}{2\sqrt{2}} \\ 0 & 0 & \frac{\lambda_d \Lambda_d v_d^2 - \lambda_u \Lambda_u v_u^2}{2\sqrt{2}} & m_T^2 + \frac{\Lambda_d^2 v_d^2 + \Lambda_u^2 v_u^2}{4} \end{pmatrix}, \quad (5)$$

4

and is diagonalized by unitary matrix Z^A

$$Z^A \mathcal{M}_{A^0}^2 (Z^A)^\dagger. \quad (6)$$

In the weak basis $(\phi_d, \phi_u, \phi_S, \phi_T)$, the scalar Higgs boson mass matrix is given by

$$\mathcal{M}_h^2 = \begin{pmatrix} \mathcal{M}_{11} & \mathcal{M}_{21}^T \\ \mathcal{M}_{21} & \mathcal{M}_{22} \end{pmatrix}, \quad (7)$$

where the submatrices ($c_\beta = \cos\beta$, $s_\beta = \sin\beta$) are

$$\begin{aligned} \mathcal{M}_{11} &= \begin{pmatrix} m_Z^2 c_\beta^2 + m_A^2 s_\beta^2 & -(m_Z^2 + m_A^2) s_\beta c_\beta \\ -(m_Z^2 + m_A^2) s_\beta c_\beta & m_Z^2 s_\beta^2 + m_A^2 c_\beta^2 \end{pmatrix}, \\ \mathcal{M}_{21} &= \begin{pmatrix} v_d(\sqrt{2}\lambda_d \mu_d^{eff,+} - g_1 M_B^D) & v_u(\sqrt{2}\lambda_u \mu_u^{eff,-} + g_1 M_B^D) \\ v_d(\Lambda_d \mu_d^{eff,+} + g_2 M_W^D) & -v_u(\Lambda_u \mu_u^{eff,1} + g_2 M_W^D) \end{pmatrix}, \\ \mathcal{M}_{22} &= \begin{pmatrix} 4(M_B^D)^2 + m_S^2 + \frac{\lambda_d^2 v_d^2 + \lambda_u^2 v_u^2}{2} & \frac{\lambda_d \Lambda_d v_d^2 - \lambda_u \Lambda_u v_u^2}{2\sqrt{2}} \\ \frac{\lambda_d \Lambda_d v_d^2 - \lambda_u \Lambda_u v_u^2}{2\sqrt{2}} & 4(M_W^D)^2 + m_T^2 + \frac{\Lambda_d^2 v_d^2 + \Lambda_u^2 v_u^2}{4} \end{pmatrix}, \end{aligned}$$

and is diagonalized by unitary matrix Z^h

$$Z^h \mathcal{M}_h^2 (Z^h)^\dagger. \quad (8)$$

The modified μ_i parameters are given by

$$\begin{aligned} \mu_d^{eff,+} &= \frac{1}{2} \Lambda_d v_T + \frac{1}{\sqrt{2}} \lambda_d v_S + \mu_d, \\ \mu_u^{eff,-} &= -\frac{1}{2} \Lambda_u v_T + \frac{1}{\sqrt{2}} \lambda_u v_S + \mu_u. \end{aligned}$$

The v_T and v_S are vacuum expectation values of \hat{T} and \hat{S} which carry zero R -charge.

The relevant Lagrangian for $l_\alpha \rightarrow 3l_\beta$ can be written as ²⁹

$$\mathcal{L}_{LFV} = \mathcal{L}_{ll\gamma} + \mathcal{L}_{4l}. \quad (9)$$

The $ll\gamma$ interaction is given by

$$\mathcal{L}_{ll\gamma} = e \bar{l}_\beta [\gamma^\mu (K_1^L P_L + K_1^R P_R) + i m_{l_\alpha} \sigma^{\mu\nu} q_\nu (K_2^L P_L + K_2^R P_R)] l_\alpha A_\mu + h.c.. \quad (10)$$

The general $4l$ 4-fermion interaction Lagrangian can be written as

$$\mathcal{L}_{4l} = A_{XY}^I \bar{l}_\beta \Gamma_I P_X l_\alpha \bar{l}_\beta \Gamma_I P_Y l_\beta + h.c., \quad (11)$$

where $I = \{S, V, T\}$, $X, Y = \{L, R\}$, $\Gamma_S = 1$, $\Gamma_V = \gamma_\mu$ and $\Gamma_T = \sigma_{\mu\nu}$.

The Higgs mediated diagrams contributing to $l_\alpha \rightarrow 3l_\beta$ in MRSSM are presented in Fig.1. The coefficients in Fig.1 (a,b) are calculated by

$$\begin{aligned} A_{XY}^S &= \frac{-1}{M_H^2} C_X^1 C_Y^4 (C_X^2, C_X^3 \mathcal{B}_0(0, M_2, M_1) + (C_X^2 C_X^3 M_1 M_2 + C_X^2 C_X^3, M_1 m_{l_\alpha} \\ &+ C_X^2, C_X^3 M_3^2) \mathcal{C}_0 + m_{l_\alpha} (C_X^2 C_X^3, M_1 + C_X^2, C_X^3 m_{l_\alpha} + C_X^2, C_X^3, M_2) \mathcal{C}_1), \quad (12) \end{aligned}$$

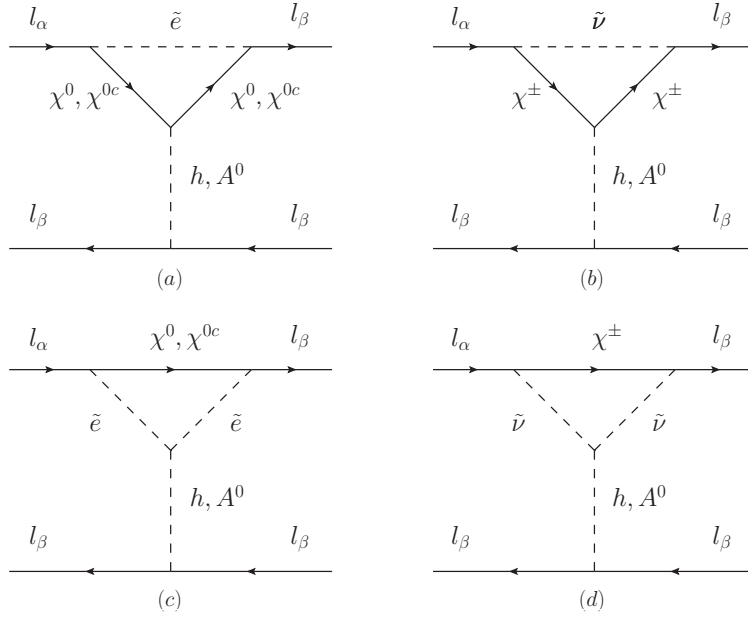


Fig. 1. Higgs penguin diagrams contributing to $l_\alpha \rightarrow 3l_\beta$ in MRSSM.

where M_H denote m_h or m_{A^0} . The symbols M_1 , M_2 and M_3 denote masses of particles in internal lines. The symbols $X'(Y')$ are defined as

$$X'(Y') = \begin{cases} L, & \text{when } X(Y) = R, \\ R, & \text{when } X(Y) = L. \end{cases}$$

Here and following, \mathcal{B} , \mathcal{C}_0 and \mathcal{C}_1 denote the Passarino-Veltman integrals, where the masses of outgoing leptons are set as zero. The explicit expressions of these integrals will be introduced later on. The couplings C_X^4 are identical in Fig.1(a-d),

$$\begin{aligned} C_L^4 &= C_R^4 = -\frac{i}{\sqrt{2}} Y_{l_\beta} Z_{l1}^h, \quad h \text{ mediated diagrams,} \\ C_L^4 &= -C_R^4 = \frac{1}{\sqrt{2}} Y_{l_\beta} Z_{l1}^{A^0}, \quad A^0 \text{ mediated diagrams,} \end{aligned} \quad (13)$$

however other couplings are defined different for each diagram. For h and χ^0 medi-

ated diagram in Fig.1(a), the relevant couplings and masses denotation are

$$\begin{aligned}
 C_L^1 &= -i\sqrt{2}N_{i1}^{1*}Z_{k(3+\beta)}^{E*}, C_R^1 = -iY_{l\beta}Z_{k(3+\beta)}^{E*}N_{i3}^2, \\
 C_L^2 &= \frac{i}{2}(-g_2N_{j2}^{1*}N_{i3}^{2*}Z_{l1}^h - \sqrt{2}\lambda_uN_{j4}^{1*}N_{i1}^{2*}Z_{l2}^h + \Lambda_uN_{j4}^{1*}N_{i2}^{2*}Z_{l2}^h + g_2N_{j2}^{1*}N_{i4}^{2*}Z_{l2}^h \\
 &\quad + g_1N_{j1}^{1*}(N_{i3}^{2*}Z_{l1}^h - N_{i4}^{2*}Z_{l2}^h) - \sqrt{2}\lambda_uN_{j4}^{1*}N_{i4}^{2*}Z_{l3}^h + \Lambda_uN_{j4}^{1*}N_{i4}^{2*}Z_{l4}^h \\
 &\quad + N_{j3}^{1*}(\Lambda_dN_{i2}^{2*}Z_{l1}^h + N_{i3}^{2*}(\Lambda_dZ_{l4}^h + \sqrt{2}\lambda_dZ_{l3}^h) + \sqrt{2}\lambda_dN_{i1}^{2*}Z_{l1}^h)), \\
 C_R^2 &= \frac{i}{2}(\Lambda_dZ_{l1}^hN_{i3}^1N_{j2}^2 + \Lambda_uZ_{l2}^hN_{i4}^1N_{j2}^2 + g_1Z_{l1}^hN_{i1}^1N_{j3}^2 - g_2Z_{l2}^hN_{i2}^1N_{j3}^2 \\
 &\quad + \Lambda_dZ_{l4}^hN_{i3}^1N_{j3}^2 + \sqrt{2}\Lambda_dN_{i3}^1(Z_{l1}^hN_{j1}^2 + Z_{l3}^hN_{j3}^2) - g_1Z_{l2}^hN_{i1}^1N_{j4}^2 \\
 &\quad + g_2Z_{l2}^hN_{i2}^1N_{j4}^2 + \Lambda_uZ_{l4}^hN_{i4}^1N_{j4}^2 - \sqrt{2}\Lambda_uN_{i4}^1(Z_{l2}^hN_{j1}^2 + Z_{l3}^hN_{j4}^2)), \\
 C_L^3 &= -iN_{j3}^{2*}Y_{l\alpha}Z_{k(3+\alpha)}^E, C_R^3 = -i\sqrt{2}g_1Z_{k(3+\alpha)}^EN_{j1}^1, \\
 M_1 &= m_{\chi^0}^i, M_2 = m_{\chi^0}^j, M_3 = m_{\tilde{e}}^k.
 \end{aligned} \tag{14}$$

For A^0 and χ^0 mediated diagram in Fig.1(a), the couplings C_X^1 , C_X^3 and masses denotation are same with those in Eq.(14), the other couplings are

$$\begin{aligned}
 C_L^2 &= \frac{1}{2}(-g_2N_{j2}^{1*}N_{i3}^{2*}Z_{l1}^A + \sqrt{2}\lambda_uN_{j4}^{1*}N_{i1}^{2*}Z_{l2}^A - \Lambda_uN_{j4}^{1*}N_{i2}^{2*}Z_{l2}^A + g_2N_{j2}^{1*}N_{i4}^{2*}Z_{l2}^A \\
 &\quad + g_1N_{j1}^{1*}(N_{i4}^{2*}Z_{l2}^A - N_{i2}^{2*}Z_{l1}^A) + \sqrt{2}\lambda_uN_{j4}^{1*}N_{i4}^{2*}Z_{l3}^A - \Lambda_uN_{j4}^{1*}N_{i4}^{2*}Z_{l4}^A \\
 &\quad - N_{j3}^{1*}(\Lambda_dN_{i2}^{2*}Z_{l1}^A + N_{i3}^{2*}(\Lambda_dZ_{l4}^A + \sqrt{2}\lambda_dZ_{l3}^A) + \sqrt{2}\lambda_dN_{i1}^{2*}Z_{l1}^A)), \\
 C_R^2 &= \frac{1}{2}(\Lambda_dZ_{l1}^AN_{i3}^1N_{j2}^2 + \Lambda_uZ_{l2}^AN_{i4}^1N_{j2}^2 - g_1Z_{l1}^AN_{i1}^1N_{j3}^2 + g_2Z_{l2}^AN_{i2}^1N_{j3}^2 \\
 &\quad + \Lambda_dZ_{l4}^AN_{i3}^1N_{j3}^2 + \sqrt{2}\Lambda_dN_{i3}^1(Z_{l1}^AN_{j1}^2 + Z_{l3}^AN_{j3}^2) + g_1Z_{l2}^AN_{i1}^1N_{j4}^2 \\
 &\quad - g_2Z_{l2}^AN_{i2}^1N_{j4}^2 + \Lambda_uZ_{l4}^AN_{i4}^1N_{j4}^2 - \sqrt{2}\Lambda_uN_{i4}^1(Z_{l2}^AN_{j1}^2 + Z_{l3}^AN_{j4}^2)).
 \end{aligned} \tag{15}$$

For h and χ^{0c} mediated diagram in Fig.1(a), the couplings C_X^2 are same with those in Eq.(14), the other couplings and masses denotation are

$$\begin{aligned}
 C_L^1 &= -iN_{i3}^{2*}Z_{k\beta}^EY_{l\beta}, C_R^1 = \frac{i}{\sqrt{2}}Z_{k\beta}^{E*}(g_1N_{i1}^1 + g_2N_{i2}^1), \\
 C_L^3 &= \frac{i}{\sqrt{2}}Z_{k\alpha}^E(g_1N_{j1}^{1*} + g_2N_{j2}^{1*}), C_R^3 = -iY_{l\alpha}Z_{k\alpha}^EN_{j3}^{2*}, \\
 M_1 &= m_{\chi^{0c}}^i, M_2 = m_{\chi^{0c}}^j, M_3 = m_{\tilde{e}}^k.
 \end{aligned} \tag{16}$$

For A^0 and χ^{0c} mediated diagram in Fig.1(a), the couplings C_X^2 are same with those in Eq.(15), couplings C_X^1 , C_X^3 and masses denotation are same with those in Eq.(16).

For h and χ^\pm mediated diagram in Fig.1(b), the relevant couplings and masses

denotation are

$$\begin{aligned}
 C_L^1 &= iU_{i2}^{1*} Z_{k\beta}^V Y_{l_\beta}, C_R^1 = -ig_2 Z_{k\beta}^{V*} V_{i1}^1, \\
 C_L^2 &= \frac{-i}{2} (U_{i1}^{1*} (2g_2 V_{j1}^{1*} Z_{l4}^h + \sqrt{2}\Lambda_d V_{j2}^{1*} Z_{l1}^h) \\
 &\quad + U_{i2}^{1*} (\sqrt{2}g_2 V_{j1}^{1*} Z_{l1}^h + \sqrt{2}\lambda_d V_{j2}^{1*} Z_{l3}^h - \Lambda_d V_{j2}^{1*} Z_{l4}^h)), \\
 C_R^2 &= \frac{-i}{2} (U_{j1}^1 (2g_2 V_{i1}^1 Z_{l4}^h + \sqrt{2}\Lambda_d V_{i2}^1 Z_{l1}^h) \\
 &\quad + U_{j2}^{1*} (\sqrt{2}g_2 V_{i1}^1 Z_{l1}^h + \sqrt{2}\lambda_d V_{i2}^1 Z_{l3}^h - \Lambda_d V_{i2}^1 Z_{l4}^h)), \\
 C_L^3 &= -ig_2 V_{j1}^{1*} Z_{k\alpha}^V, C_R^3 = iY_{l_\alpha} Z_{k\alpha}^V U_{j2}^1, \\
 M_1 &= m_{\chi^\pm}^i, M_2 = m_{\chi^\pm}^j, M_3 = m_{\tilde{\nu}}^k.
 \end{aligned} \tag{17}$$

For A^0 and χ^\pm mediated diagram in Fig.1(b), the couplings C_X^1 , C_X^3 and masses denotation are same with those in Eq.(17), and the remaining couplings are

$$\begin{aligned}
 C_L^2 &= \frac{-1}{2} (U_{i1}^{1*} (2g_2 V_{j1}^{1*} Z_{l4}^A + \sqrt{2}\Lambda_d V_{j2}^{1*} Z_{l1}^A) \\
 &\quad + U_{i2}^{1*} (\sqrt{2}g_2 V_{j1}^{1*} Z_{l1}^A - \sqrt{2}\lambda_d V_{j2}^{1*} Z_{l3}^A + \Lambda_d V_{j2}^{1*} Z_{l4}^A)), \\
 C_R^2 &= \frac{1}{2} (U_{j1}^1 (2g_2 V_{i1}^1 Z_{l4}^A - \sqrt{2}\Lambda_d V_{i2}^1 Z_{l1}^A) \\
 &\quad + U_{j2}^{1*} (\sqrt{2}g_2 V_{i1}^1 Z_{l1}^A - \sqrt{2}\lambda_d V_{i2}^1 Z_{l3}^A + \Lambda_d V_{i2}^1 Z_{l4}^A)).
 \end{aligned} \tag{18}$$

The coefficients in Fig.1 (c,d) are calculated by

$$A_{XY}^S = \frac{1}{M_H^2} C_X^1 C^2 C_Y^4 (C_X^3 m_{l_\alpha} C_1 - C_X^3 M_3 C_0). \tag{19}$$

For h and χ^0 mediated diagram in Fig.1 (c), the couplings C_X^1 and C_X^3 are same with those in Eq.(14) except an interchange of subscripts ($i \leftrightarrow k, j \leftrightarrow k$). The remaining coupling C^2 and masses denotation are

$$\begin{aligned}
 C^2 &= \sum_{a=1,2,3} \frac{i}{4} (2(-2v_d Z_{i(3+a)}^{E*} Y_{l_a} Y_{l_a} Z_{j(3+a)}^E Z_{l1}^h - 2v_d Z_{ia}^{E*} Y_{l_a} Y_{l_a} Z_{ja}^E Z_{l1}^h) \\
 &\quad + g_1 Z_{i(3+\beta)}^{E*} Z_{j(3+\beta)}^E (g_1 v_d Z_{l1}^h - g_1 v_u Z_{l2}^h - 4M_D^B Z_{l3}^h)) + Z_{ia}^{E*} Z_{ja}^{E*} \\
 &\quad \times (4(g_1 M_D^B Z_{l3}^h + g_2 M_D^W Z_{l4}^h) + (g_2^2 - g_1^2) v_d Z_{l1}^h + (g_1^2 - g_2^2) v_u Z_{l2}^h), \\
 M_1 &= m_{\tilde{e}}^i, M_2 = m_{\tilde{e}}^j, M_3 = m_{\chi^0}^k.
 \end{aligned} \tag{20}$$

For h and χ^{0c} mediated diagram in Fig.1 (c), the couplings C_X^1 and C_X^3 are same with those in Eq.(16) except an interchange of subscripts ($i \leftrightarrow k, j \leftrightarrow k$). The couplings C^2 and masses denotation are same with that Eq.(20). For A^0 mediated diagrams in Fig.1 (c), the contribution is zero as we have assumed both M_D^W and M_D^B are real numbers in the coupling of $A^0 \tilde{e} \tilde{e}$ interaction.

For h and χ^\pm mediated diagram in Fig.1 (d), the couplings C_X^1 and C_X^3 are same with those in Eq.(17) except an interchange of subscripts ($i \leftrightarrow k, j \leftrightarrow k$). The

remaining coupling C^2 and mass denotation are

$$C^2 = \frac{i}{4} \delta^{ij} (4(g_1 M_D^B Z_{i3}^h - g_2 M_D^W Z_{i4}^h) - (g_1^2 + g_2^2)(v_d Z_{i1}^h - v_u Z_{i2}^h)),$$

$$M_1 = m_{\tilde{\nu}}^i, M_2 = m_{\tilde{\nu}}^j, M_3 = m_{\chi^\pm}^k. \quad (21)$$

For A^0 mediated diagrams in Fig.1 (d), the contribution is also zero since we have assumed both M_D^W and M_D^B are real numbers in the coupling of $A^0 \tilde{\nu} \tilde{\nu}$ interaction.

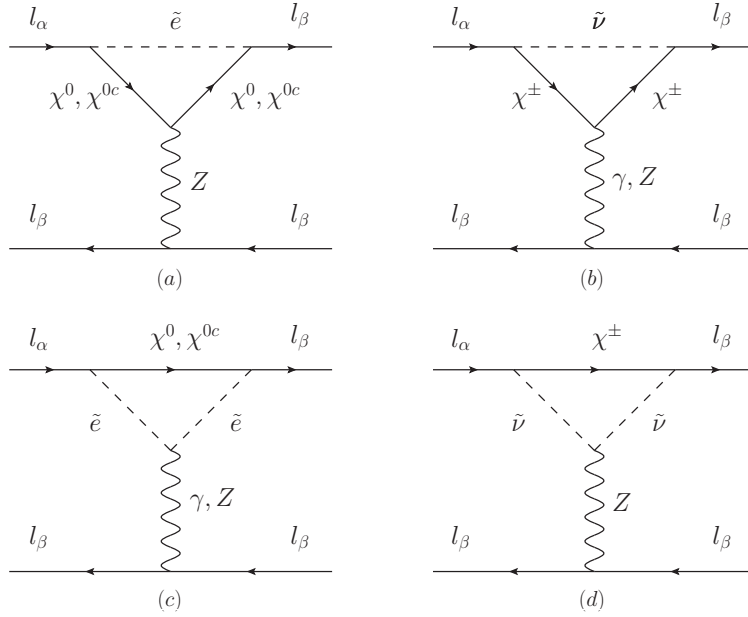


Fig. 2. Photon and Z penguin diagrams contributing to $l_\alpha \rightarrow 3l_\beta$ in MRSSM.

The photon and Z boson mediated diagrams contributing to $l_\alpha \rightarrow 3l_\beta$ in MRSSM are presented in Fig.2. The coefficients in Fig.2 (a,b) are calculated by

$$A_{XY}^V = \frac{-1}{M_Z^2} C_X^1 C_Y^4 (C_X^2 C_X^3 \mathcal{B}_0(0, M_2, M_1) + (C_X^2 C_X^3 M_3^2 - C_X^2 C_X^3 M_1 M_2 - C_X^2 C_X^3 M_1 m_{l_\alpha}) \mathcal{C}_0 - C_X^2 C_X^3 M_1 m_{l_\alpha} \mathcal{C}_1 - 2C_X^2 C_X^3 \mathcal{C}_{00} + C_X^2 C_X^3 m_{l_\alpha}^2 \mathcal{C}_1 + C_X^2 C_X^3 M_2 m_{l_\alpha} \mathcal{C}_1), \quad (22)$$

where C_X^4 are identical in Fig.2(a-d),

$$C_L^4 = \frac{i}{2} (g_2 c_w - g_1 s_w), C_R^4 = -i g_1 s_w. \quad (23)$$

For χ^0 mediated diagram in Fig.2 (a), the couplings C_X^1 , C_X^3 and masses denotation

are same with those in Eq.(14). The remaining couplings are

$$\begin{aligned} C_L^2 &= \frac{i}{2}(g_1 s_w + g_2 c_w)(N_{j3}^{1*} N_{i3}^1 - N_{j4}^{1*} N_{i4}^1), \\ C_R^2 &= \frac{i}{2}(g_1 s_w + g_2 c_w)(N_{i3}^{2*} N_{j3}^2 - N_{i4}^{2*} N_{j4}^2). \end{aligned} \quad (24)$$

For χ^{0c} mediated diagram in Fig.2 (a), the couplings C_X^1 , C_X^3 and masses denotation are same with those in Eq.(16). The remaining couplings C_X^2 are same with those in Eq.(24). For χ^\pm mediated diagram in Fig.2 (b), the couplings C_X^1 , C_X^3 and masses denotation are same with those in Eq.(17). The remaining couplings are

$$\begin{aligned} C_L^2 &= \frac{-i}{2}(2g_2 c_w V_{j1}^{1*} V_{i1}^1 + (g_2 c_w - g_1 s_w) V_{j2}^{1*} V_{i1}^1), \\ C_R^2 &= \frac{-i}{2}(2g_2 c_w U_{i1}^{1*} U_{j1}^1 + (g_2 c_w - g_1 s_w) U_{i2}^{1*} U_{j2}^1). \end{aligned} \quad (25)$$

The coefficients in Fig.2 (c,d) are calculated by

$$A_{XY}^V = \frac{1}{M_Z^2} C_X^1 C_X^2 C_X^3 C_Y^4 C_{00}. \quad (26)$$

For χ^0 mediated diagram in Fig.2 (c), the couplings C_X^1 and C_X^3 are same with those in Eq.(14) except an interchange of subscripts ($i \leftrightarrow k, j \leftrightarrow k$). The masses denotation are same with those in Eq.(20), and the remaining coupling C^2 is

$$C^2 = \sum_{a=1,2,3} \frac{i}{2} (-2g_1 s_w Z_{i(3+a)}^{E*} Z_{j(3+a)}^E + (g_2 c_w - g_1 s_w) Z_{ia}^{E*} Z_{ja}^E). \quad (27)$$

For χ^{0c} mediated diagram in Fig.2 (c), the couplings C_X^1 and C_X^3 are same with those in Eq.(16) except an interchange of subscripts ($i \leftrightarrow k, j \leftrightarrow k$). The masses denotation are same with those in Eq.(20). The remaining coupling C^2 is same with that in Eq.(27). For χ^\pm mediated diagram in Fig.2 (d), the couplings C_X^1 and C_X^3 are same with those in Eq.(17) except an interchange of subscripts ($i \leftrightarrow k, j \leftrightarrow k$). The masses denotation are same with those in Eq.(21). The remaining coupling C^2 is $C^2 = -\frac{i}{2} \delta^{ij} (g_1 s_w + g_2 c_w)$.

The K_1^X and K_2^X coefficients in Fig.2 (b) are calculated by

$$\begin{aligned} K_1^X &= \frac{I}{16\pi^2} C_X^1 C_X^2 C_X^3 C_{12}, \\ K_2^X &= \frac{-I}{16\pi^2 m_{l_\alpha}} C_X^1 (C_X^2 ((C_X^3 M_2 + C_X^3 m_{l_\alpha}) C_1 \\ &\quad + C_X^3 m_{l_\alpha} (C_{12} + C_{11})) + C_X^2 C_X^3 M_1 C_2). \end{aligned} \quad (28)$$

The couplings C_X^1 , C_X^3 and masses denotation are same with those in Eq.(17), and $C_X^2 = -ie\delta^{ij}$.

The coefficient K_1^X in Fig.2 (c) is zero, and K_2^X is calculated by

$$\begin{aligned} K_2^X &= \frac{I}{32\pi^2 m_{l_\alpha}} C_X^1 C^2 (C_X^3 m_{l_\alpha} (2C_{12} + 2C_{11} \\ &\quad + C_1) - C_X^3 M_3 (C_0 + 2C_1 + 2C_2)). \end{aligned} \quad (29)$$

For χ^{0c} mediated diagram in Fig.2 (c), the couplings C_X^1 and C_X^3 are same with those in Eq.(16) except an interchange of subscripts ($i \leftrightarrow k, j \leftrightarrow k$). The masses denotation are same with those in Eq.(20). The remaining coupling C^2 is $ie\delta^{ij}$. For χ^\pm mediated diagram in Fig.2 (d), the couplings C_X^1 and C_X^3 are same with those in Eq.(17) except an interchange of subscripts ($i \leftrightarrow k, j \leftrightarrow k$). The masses denotation are same with those in Eq.(21). The remaining coupling C^2 is $ie\delta^{ij}$.

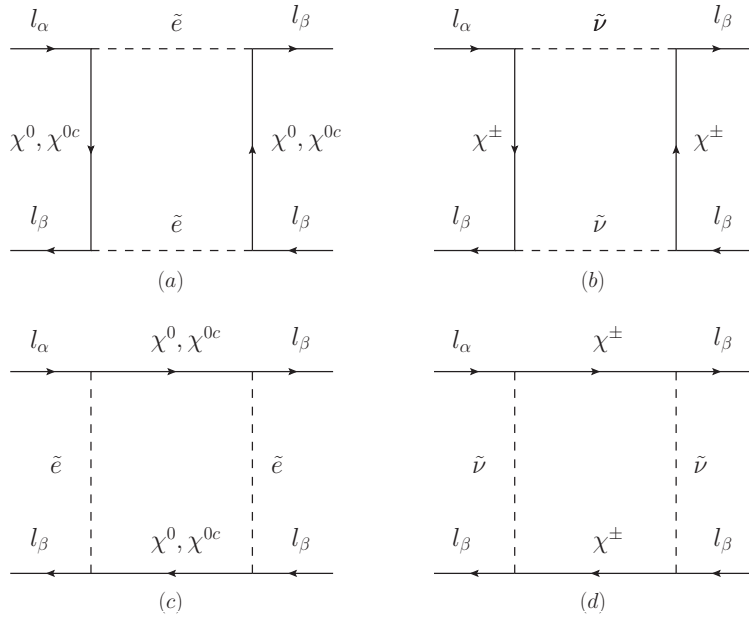


Fig. 3. Box diagrams contributing to $l_\alpha \rightarrow 3l_\beta$ in MRSSM.

The box diagrams contributing to $l_\alpha \rightarrow 3l_\beta$ in MRSSM are presented in Fig.2. The coefficients in Fig.3 (a,b) are calculated by

$$\begin{aligned} A_{XY}^S &= C_X^1 C_X^2 C_Y^3 M_1 ((C_Y^4 M_3 - C_Y^4 m_{l_\alpha}) \mathcal{D}_0 - C_Y^4 m_{l_\alpha} (\mathcal{D}_2 + \mathcal{D}_1)), \\ A_{XY}^V &= C_X^1 C_X^2 C_Y^3 C_Y^4 \mathcal{D}_{00}. \end{aligned} \quad (30)$$

For two χ^0 mediated diagram in Fig.3 (a), the couplings are

$$\begin{aligned} C_L^1 &= -i\sqrt{2}g_1 N_{i1}^{1*} Z_{k(3+\beta)}^{E*}, C_R^1 = -iY_{l_\beta} Z_{k(3+\beta)}^E N_{i3}^2, \\ C_L^2 &= -iN_{i3}^{2*} Y_{l_\beta} Z_{l(3+\beta)}^E, C_R^2 = -i\sqrt{2}g_1 Z_{l(3+\beta)}^E N_{i1}^1. \end{aligned} \quad (31)$$

The couplings C_X^3 are same with C_X^1 in Eq.(31) with interchange of subscripts ($i \leftrightarrow j, k \leftrightarrow l$), C_X^4 are same with C_X^2 in Eq.(31) with index exchange ($i \leftrightarrow j, k \leftrightarrow$

$l, \beta \leftrightarrow \alpha$). For two χ^{0c} mediated diagram in Fig.3 (a), the couplings are

$$\begin{aligned} C_L^1 &= -iY_{l\beta} N_{i3}^{2*} Z_{k\beta}^{E*}, C_R^1 = \frac{i}{\sqrt{2}} Z_{k\beta}^{E*} (g_1 N_{i1}^1 + g_2 N_{i2}^1), \\ C_L^2 &= \frac{i}{\sqrt{2}} Z_{l\beta}^E (g_1 N_{i1}^{1*} + g_2 N_{i2}^{1*}), C_R^2 = -iY_{l\beta} Z_{l\beta}^E N_{i3}^2. \end{aligned} \quad (32)$$

The couplings C_X^3 are same with C_X^1 in Eq.(32) with interchange of subscripts ($i \leftrightarrow j, k \leftrightarrow l$), C_X^4 are same with C_X^2 in Eq.(32) with index exchange ($i \leftrightarrow j, k \leftrightarrow l, \beta \leftrightarrow \alpha$). For $\chi^0 \chi^{0c}$ mediated diagram in Fig.3 (a), the couplings C_X^1 and C_X^2 are same with those in Eq.(32), and the couplings C_X^3 and C_X^4 are same with those after Eq.(31). For $\chi^{0c} \chi^0$ mediated diagram in Fig.3 (a), the couplings C_X^1 and C_X^2 are same with those in Eq.(31), and the couplings C_X^3 and C_X^4 are same with those after Eq.(32). The masses denotation are $M_1 = m_{\chi^0}^i$, $M_2 = m_{\tilde{e}}^l$, $M_3 = m_{\chi^0}^j$ and $M_4 = m_{\tilde{e}}^k$.

For two χ^\pm mediated diagram in Fig.3 (b), the couplings and masses denotation are

$$\begin{aligned} C_L^1 &= iU_{i2}^{1*} Z_{k\beta}^V Y_{l\beta}, C_R^1 = -ig_2 Z_{k\beta}^{V*} V_{i1}^1, C_L^2 = -(C_R^1)^*(k \leftrightarrow l), \\ C_R^2 &= -(C_L^1)^*(k \leftrightarrow l), C_L^3 = -C_L^1(i \leftrightarrow j, k \leftrightarrow l), C_R^3 = -C_R^1(i \leftrightarrow j, k \leftrightarrow l), \\ C_L^4 &= -(C_R^1)^*(i \leftrightarrow j, k \leftrightarrow l, \beta \leftrightarrow \alpha), C_R^4 = -(C_L^1)^*(i \leftrightarrow j, k \leftrightarrow l, \beta \leftrightarrow \alpha). \end{aligned} \quad (33)$$

The masses denotation are $M_1 = m_{\chi^\pm}^i$, $M_2 = m_{\tilde{\nu}}^l$, $M_3 = m_{\chi^\pm}^j$ and $M_4 = m_{\tilde{\nu}}^k$.

The coefficients in Fig.3 (c,d) are calculated by

$$\begin{aligned} A_{XY}^S &= C_X^1 C_Y^2 C_Y^3 M_2 (C_X^4 M_4 \mathcal{D}_0 - C_X^4 m_{l\alpha} (\mathcal{D}_2 + \mathcal{D}_1)), \\ A_{XY}^V &= C_X^1 C_Y^2 C_Y^3 C_X^4 \mathcal{D}_{00}. \end{aligned} \quad (34)$$

The couplings C_X^1 , C_X^2 , C_X^3 and C_X^4 correspond to diagrams in Fig.3 (c,d) are same as those in Fig.3 (a,b) respectively, where following interchanges of subscripts should be made: ($i \leftrightarrow k$), ($i \leftrightarrow l$), ($j \leftrightarrow l$) and ($j \leftrightarrow k$). The masses notation in Fig.3 (c) are $M_1 = m_{\tilde{e}}^i$, $M_2 = m_{\chi^0}^l$, $M_3 = m_{\tilde{e}}^j$ and $M_4 = m_{\chi^0}^k$. The masses notation in Fig.3 (d) are $M_1 = m_{\tilde{\nu}}^i$, $M_2 = m_{\chi^\pm}^l$, $M_3 = m_{\tilde{\nu}}^j$ and $M_4 = m_{\chi^\pm}^k$.

Using the Wilson coefficients in Eqs.(10, 11), the decay width $\Gamma(l_\alpha \rightarrow 3l_\beta)$ is given by ²⁹

$$\begin{aligned} \Gamma(l_\alpha \rightarrow 3l_\beta) &= \frac{m_{l_\alpha}^5}{512\pi^3} [e^4 (|K_2^L|^2 + |K_2^R|^2) (\frac{16}{3} \ln \frac{m_{l_1}}{m_{l_2}} - \frac{22}{3}) + \frac{1}{24} (|A_{LL}^S|^2 + |A_{RR}^S|^2) \\ &+ \frac{1}{12} (|A_{LR}^S|^2 + |A_{RL}^S|^2) + \frac{2}{3} (|\hat{A}_{LL}^V|^2 + |\hat{A}_{RR}^V|^2) + \frac{1}{3} (|\hat{A}_{LR}^V|^2 + |\hat{A}_{RL}^V|^2) \\ &+ 6(|A_{LL}^T|^2 + |A_{RR}^T|^2) + \frac{2e^2}{3} \text{Re}(K_2^L A_{RL}^{S*} + K_2^R A_{LR}^{S*}) - \frac{4e^2}{3} \text{Re}(K_2^L \hat{A}_{RL}^{V*} \\ &+ K_2^R \hat{A}_{LR}^{V*}) - \frac{8e^2}{3} \text{Re}(K_2^L \hat{A}_{RR}^{V*} + K_2^R \hat{A}_{LL}^{V*}) - \text{Re}(A_{LL}^S A_{LL}^{T*} + A_{RR}^S A_{RR}^{T*}) \\ &- \frac{1}{3} \text{Re}(A_{LR}^S \hat{A}_{LR}^{V*} + A_{RL}^S \hat{A}_{RL}^{T*})]. \end{aligned} \quad (35)$$

As mentioned earlier, loop integrals are given in term of Passarino-Veltman functions³⁰,

$$\begin{aligned}\mathcal{C}_{(0,1,\dots,12)} &= \frac{i}{16\pi^2} \mathcal{C}_{(0,1,\dots,12)}(m_{l_\alpha}^2, 0, 0; M_3, M_1, M_2), \\ \mathcal{D}_{(0,1,\dots,00)} &= \frac{i}{16\pi^2} \mathcal{D}_{(0,1,\dots,00)}(0, 0, m_{l_\alpha}^2, 0, ; m_{l_\alpha}^2, 0; M_1, M_2, M_3, M_4).\end{aligned}\quad (36)$$

The explicit expressions of these loop integrals are given in Refs.^{31,32,33} and \overline{MS} scheme is used to delete the infinite terms. These loop integrals can be calculated through the Mathematica package Package-X³⁴ and a link to Collier which is a fortran library for the numerical evaluation of one-loop scalar and tensor integrals³⁵.

3. Numerical Analysis

In the numerical analysis, we will use the benchmark point in Refs.^{6,19,20} as the default values in our parameter setup, where the soft breaking terms m_l^2 , m_r^2 are diagonal. In this work, the off-diagonal entries of the soft breaking terms m_l^2 , m_r^2 are parameterized by mass insertion as in Ref.^{36,37,38},

$$\begin{aligned}(m_l^2)^{IJ} &= \delta_l^{IJ} \sqrt{(m_l^2)^{II} (m_l^2)^{JJ}}, \\ (m_r^2)^{IJ} &= \delta_r^{IJ} \sqrt{(m_r^2)^{II} (m_r^2)^{JJ}},\end{aligned}\quad (37)$$

where $I, J = \{1, 2, 3\}$. We also assume $\delta_l^{IJ} = \delta_r^{IJ} = \delta^{IJ}$. In the following, we will use LFV decays $l_\alpha \rightarrow l_\beta \gamma$ to constrain the parameters δ^{IJ} and the explicit expression can be found in Ref.²⁰. For the values of $\mu_u(\mu_d)$, M_D^W and M_D^B , we have considered the constraints from theoretical valid regions in Ref.³⁹ and the experimental bounds from ATLAS⁴⁰. The large value of $|v_T|$ is excluded by measurement of W mass cause the vev v_T of the $SU(2)_L$ triplet field T^0 gives a correction to W mass through⁴

$$m_W^2 = \frac{1}{4} g_2^2 v^2 + g_2^2 v_T^2, \quad (38)$$

with $v^2 = v_u^2 + v_d^2$. Then, the numerical values in our parameter setup are

$$\begin{aligned}\alpha_{em}(m_Z) &= 1/137, m_Z = 91.1876 \text{ GeV}, m_W = 80.379 \text{ GeV}, \\ \sin^2 \theta_W &= 0.23129, m_e = 0.510 \text{ MeV}, m_\mu = 105.6 \text{ MeV}, m_\tau = 1.776 \text{ GeV}, \\ \tan \beta &= 40, B_\mu = 300^2 \text{ GeV}^2, \lambda_d = -\lambda_u = 0.15, \Lambda_d = -1.0, \Lambda_u = -1.15, \\ v_S &= -0.14 \text{ GeV}, v_T = -0.34 \text{ GeV}, M_D^B = M_D^W = \mu_d = \mu_u = 600 \text{ GeV}, \\ m_T^2 &= 3000^2 \text{ GeV}^2, m_l^2 = m_r^2 = 1000^2 \text{ GeV}^2.\end{aligned}\quad (39)$$

Taking data in Eq.(39) and $\delta^{13} = \delta^{23} = 0$, we display the theoretical prediction of $\text{Br}(\mu \rightarrow 3e)$ versus $\text{Log}_{10}[\delta^{12}]$ in MRSSM in Fig.4, where the contributions from total diagrams (solid line), Higgs penguins (dot line), γ penguins (dash line), Z penguins (dash dot line) and box diagrams (short dash line) are listed. We observe that a linear relationship is displayed between different predictions for $\text{Br}(\mu \rightarrow 3e)$

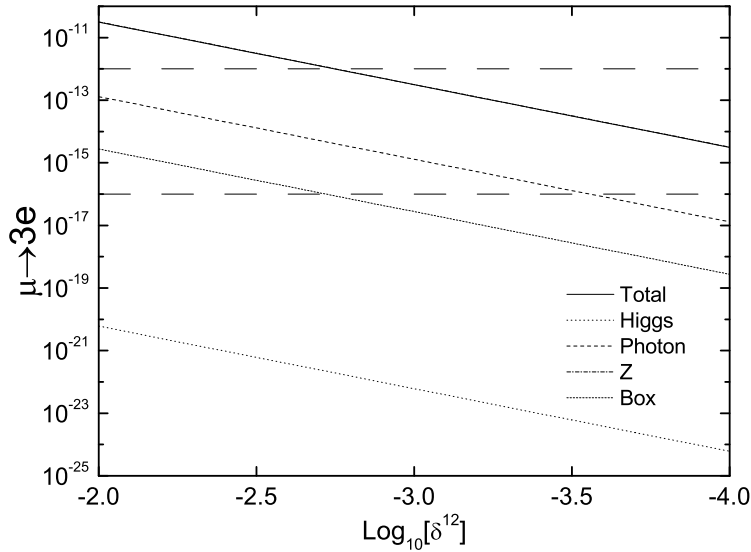


Fig. 4. $\text{Br}(\mu \rightarrow 3e)$ vary as a function of $\text{Log}_{10}[\delta^{12}]$ in MRSSM, where the contributions from total diagrams (solid line), Higgs penguins (dot line), γ penguins (dash line), Z penguins (dash dot line) and box diagrams (short dash line) are listed. The upper horizontal dash line denotes the experimental upper limit and the lower horizontal dash line denotes the future experimental sensitivity.

and $\text{Log}_{10}[\delta^{12}]$ in logarithmic scale, which show a great dependence of $\text{Br}(\mu \rightarrow 3e)$ on δ^{12} . It shows that Higgs contribution is negligible ($\mathcal{O}(10^{-25} - 10^{-21})$), which is ten orders of magnitude below the total prediction for $\text{Br}(\mu \rightarrow 3e)$. The box contribution ($\mathcal{O}(10^{-19} - 10^{-15})$) and γ contribution ($\mathcal{O}(10^{-16} - 10^{-13})$) are about four and two orders of magnitude below the total prediction respectively. The contribution from Z diagrams takes an important role in prediction for $\text{Br}(\mu \rightarrow 3e)$ and is too close to the total prediction to distinguish them in Fig.4. Considering the discussion in Ref.²⁰, the value of δ^{13} is about 10^{-1} . Then, the total prediction for $\text{Br}(\mu \rightarrow 3e)$ ($\mathcal{O}(10^{-9})$) is one order of magnitude below the current experimental limit in Table.1.

Taking data in Eq.(39) and $\delta^{12} = \delta^{23} = 0$, we display the theoretical prediction of $\text{Br}(\tau \rightarrow 3e)$ versus $\text{Log}_{10}[\delta^{13}]$ in MRSSM in Fig.5, where the contributions from total diagrams (solid line), Higgs penguins (dot line), γ penguins (dash line), Z penguins (dash dot line) and box diagrams (short dash line) are listed. We observe that a linear relationship is displayed between different prediction for $\text{Br}(\tau \rightarrow 3e)$ and $\text{Log}_{10}[\delta^{12}]$ in logarithmic scale, which shows the great dependence of $\text{Br}(\tau \rightarrow 3e)$ on δ^{12} . It shows that Higgs contribution is negligible ($\mathcal{O}(10^{-21} - 10^{-15})$), which is eight orders of magnitude below the total prediction. The box contribution ($\mathcal{O}(10^{-18} - 10^{-11})$) and γ contribution ($\mathcal{O}(10^{-15} - 10^{-9})$) are about four and two orders of magnitude below the total prediction respectively. The contribution from Z diagrams is very close to the total prediction and takes an important

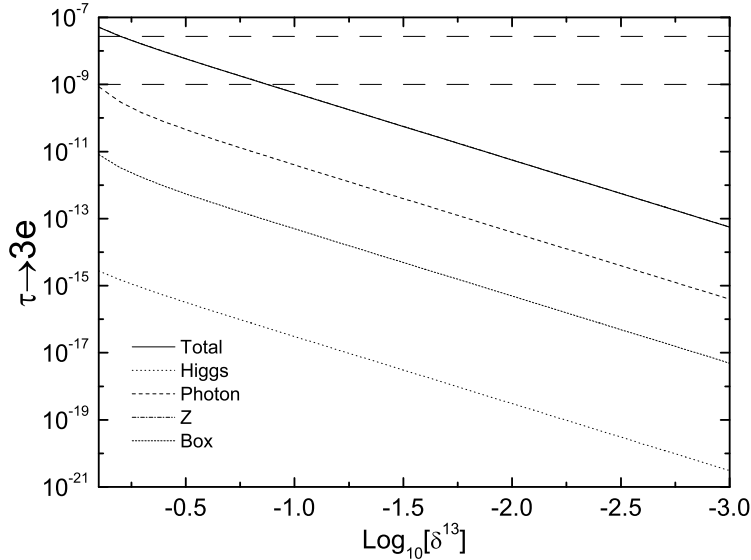


Fig. 5. $Br(\tau \rightarrow 3e)$ vary as a function of $\text{Log}_{10}[\delta^{13}]$ in MRSSM, where the contributions from total diagrams (solid line), Higgs penguins (dot line), γ penguins (dash line), Z penguins (dash dot line) and box diagrams (short dash line) are listed. The upper horizontal dash line denotes the experimental upper limit and the lower horizontal dash line denotes the future experimental sensitivity.

role in $Br(\tau \rightarrow 3e)$, which is hard to distinguish them in Fig.5. Considering the discussion in Ref.²⁰, the value of δ^{13} is about 10^{-3} . Then, the total prediction $Br(\tau \rightarrow 3e)(\mathcal{O}(10^{-9}))$ is one order of magnitude below the current experimental limit in Table.1.

Taking data in Eq.(39) and $\delta^{12} = \delta^{13} = 0$, we display the theoretical prediction of $Br(\tau \rightarrow 3\mu)$ versus $\text{Log}_{10}[\delta^{23}]$ in MRSSM in Fig.6, where the contributions from total diagrams (solid line), Higgs penguins (dot line), γ penguins (dash line), Z penguins (dash dot line) and box diagrams (short dash line) are listed. There is also a linear relationship between different prediction for $Br(\tau \rightarrow 3\mu)$ and $\text{Log}_{10}[\delta^{23}]$ in logarithmic scale, which shows the great dependence of $Br(\tau \rightarrow 3\mu)$ on δ^{23} . Compare with other three contributions, it shows that box contribution is negligible ($\mathcal{O}(10^{-18} - 10^{-12})$). The Higgs contribution ($\mathcal{O}(10^{-17} - 10^{-10})$) and γ contribution ($\mathcal{O}(10^{-16} - 10^{-10})$) are about two orders of magnitude below the total prediction respectively. The contribution from Z penguins is very close to the total prediction and takes an important role in $Br(\tau \rightarrow 3\mu)$, which is hard to distinguish them in Fig.6. Considering the discussion in Ref.²⁰, the value of δ^{23} is about 10^{-3} . Then, the total prediction for $Br(\tau \rightarrow 3\mu)(\mathcal{O}(10^{-10}))$ is two orders of magnitude below the current experimental limit in Table.1.

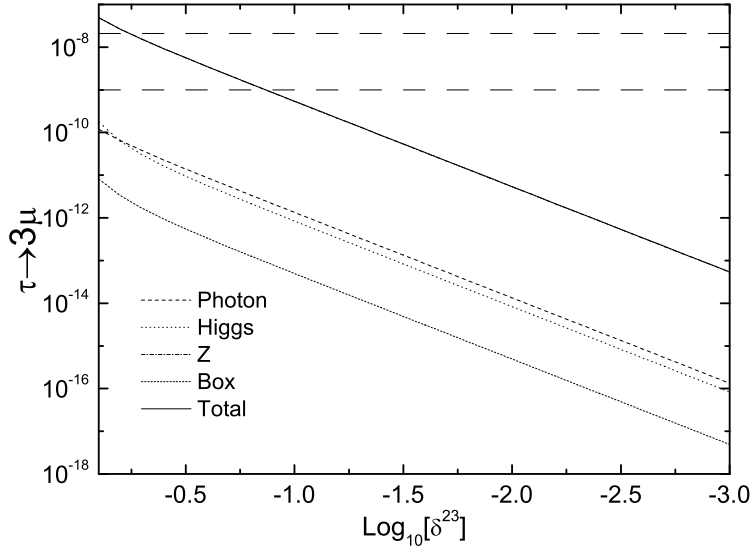


Fig. 6. $Br(\tau \rightarrow 3\mu)$ vary as a function of $\text{Log}_{10}[\delta^{23}]$ in MRSSM, where the contributions from total diagrams (solid line), Higgs penguins (dot line), γ penguins (dash line), Z penguins (dash dot line) and box diagrams (short dash line) are listed. The upper horizontal dash line denotes the experimental upper limit and the lower horizontal dash line denotes the future experimental sensitivity.

4. Conclusions

We have investigated the LFV processes $l_\alpha \rightarrow 3l_\beta$ in the framework of Minimal R-symmetric Supersymmetric Standard Model (MRSSM) as a function of model parameters δ^{ij} . The predictions for $Br(l_\alpha \rightarrow 3l_\beta)$ show a great dependent on off-diagonal inputs δ^{ij} . Taking account of the constraints on δ^{ij} from LFV processes $l_\alpha \rightarrow l_\beta\gamma$, all predictions for $Br(l_\alpha \rightarrow 3l_\beta)$ can be enhanced up to the current experimental limits or future experimental sensitivities. Thus, more precise measurements of $Br(l_\alpha \rightarrow l_\beta\gamma)$ and $Br(l_\alpha \rightarrow 3l_\beta)$ in experiment are in need.

Acknowledgements

The work has been supported by the Scientific Research Foundation of the Higher Education Institutions of Hebei Province with Grant No. BJ2019210, the Foundation of Baoding University with Grant No. 2018Z01, the National Natural Science Foundation of China (NNSFC) with Grants No. 11805140 and No. 11705045, the Scientific and Technological Innovation Programs of Higher Education Institutions in Shanxi with Grant No. 2017113, the Natural Science Foundation of Shanxi Province with Grant No. 201801D221021, the youth top-notch talent support program of the Hebei Province.

References

1. G. D. Kribs, E. Poppitz and N. Weiner, *Phys. Rev. D* 78 (2008) 055010.
2. P. Fayet, *Nucl. Phys. B* 90 (1975) 104.
3. A. Salam, J. Strathdee, *Nucl. Phys. B* 87 (1975) 85.
4. P. Diessner, W. Kotlarski, *PoS CORFU 2014* (2015) 079.
5. P. Diessner, J. Kalinowski, W. Kotlarski, D. Stöckinger, *Adv. High Energy Phys.* 2015 (2015) 760729.
6. P. Diessner, J. Kalinowski, W. Kotlarski, D. Stöckinger, *JHEP* 1412 (2014) 124.
7. P. Diessner, W. Kotlarski, S. Liebschner, D. Stöckinger, *JHEP* 1710 (2017) 142.
8. P. Diessner, J. Kalinowski, W. Kotlarski, D. Stöckinger, *JHEP* 1603 (2016) 007.
9. P. Diessner, G. Weiglein, *JHEP* 1907 (2019) 011.
10. A. Kumar, D. Tucker-Smith, N. Weiner, *JHEP* 1009 (2010) 111.
11. A. E. Blechman, *Mod.Phys.Lett. A* 24 (2009) 633.
12. G. D. Kribs, A. Martin, T. S. Roy, *JHEP* 0906 (2009) 042.
13. C. Frugiuele, T. Gregoire, *Phys.Rev. D* 85 (2012) 015016.
14. J. Kalinowski, *Acta Phys.Polon. B* 47 (2016) 203.
15. S. Chakraborty, A. Chakraborty, S. Raychaudhuri, *Phys.Rev. D* 94 (2016) 035014.
16. J. Braathen, M. D. Goodsell, P. Slavich, *JHEP* 1609 (2016) 045.
17. P. Athron, J.-hyeon Park, T. Steudtner, D. Stöckinger, A. Voigt, *JHEP* 1701 (2017) 079.
18. C. Alvarado, A. Delgado, A. Martin, *Phys. Rev. D* 97 (2018) 115044.
19. K.-S. Sun, J.-B. Chen, X.-Y. Yang, H.-B. Zhang, *Mod. Phys. Lett. A* 34 (2019) 1950058.
20. K.-S. Sun, J.-B. Chen, X.-Y. Yang, S.-K. Cui, *Chin. Phys. C* 43 (2019) 043101.
21. W. Kotlarski, D. Stöckinger, H. Stöckinger-Kim, *arXiv:1902.06650*.
22. U. Bellgardt et al. [SINDRUM Collaboration], *Nucl. Phys. B* 299 (1988) 1.
23. A. Blondel et al., *arXiv:1301.6113 [physics.ins-det]*.
24. K. Hayasaka et al., *Phys. Lett. B* 687, 139(2010).
25. K. Hayasaka [Belle and Belle-II Collaborations], *J. Phys. Conf. Ser.* 408 (2013) 012069.
26. B.Pontecorvo, *Zh. Eksp. Teor. Fiz. JETP* 33 (1957) 549.
27. B.Pontecorvo, *Zh. Eksp. Teor. Fiz. JETP* 34(1958) 247.
28. Z.Maki, M.Nakagawa and S.Sakata, *Prog. Theor. Phys.* 28 (1962) 870.
29. W. Porod, F. Staub, A. Vicente, *Eur.Phys.J. C* 74 (2014) 2992.
30. G. Passarino, M.J.G. Veltman, *Nucl. Phys. B* 160 (1979) 151.
31. A. Denner, S. Dittmaier, *Nucl. Phys. B* 658 (2003) 175.
32. A. Denner, S. Dittmaier, *Nucl. Phys. B* 734 (2006) 62.
33. A. Denner, *Fortsch.Phys.* 41 (1993) 307.
34. H. H. Patel, *Comput. Phys. Commun.* 197 (2015) 276.
35. A. Denner, S. Dittmaier, L. Hofer, *Comput.Phys.Commun.* 212 (2017) 220.
36. J. Rosiek, P. Chankowski, A. Dedes, S. Jager, P. Tanedo, *Comput.Phys.Commun.* 181 (2010) 2180.
37. K.-S. Sun, T.-F. Feng, T.-J. Gao, S.-M. Zhao, *Nucl.Phys. B* 865 (2012) 486.
38. H. B. Zhang, T. F. Feng, S. M. Zhao and F. Sun, *Int.J.Mod.Phys. A* 29 (2014) 1450123.
39. P. Diessner, PhD thesis, Dresden, Tech. U., 2016.
40. ATLAS collaboration. (M. Aaboud et al.), *Phys.Rev. D* 98 (2018) 092012.